Dark and antidark soliton interactions in the nonlocal nonlinear Schrödinger equation with the self-induced parity-time-symmetric potential

Min Li[1,*] and Tao Xu[2,†]

[1]*Department of Mathematics and Physics, North China Electric Power University, Beijing 102206, China*

[2]*College of Science, China University of Petroleum, Beijing 102249, China*

(Received 21 December 2014; published 5 March 2015)

Via the Nth Darboux transformation, a chain of nonsingular localized-wave solutions is derived for a nonlocal nonlinear Schrödinger equation with the self-induced parity-time ($\mathcal{PT}$) -symmetric potential. It is found that the Nth iterated solution in general exhibits a variety of elastic interactions among $2N$ solitons on a continuous-wave background and each interacting soliton could be the dark or antidark type. The interactions with an arbitrary odd number of solitons can also be obtained under different degenerate conditions. With $N = 1$ and 2, the two-soliton and four-soliton interactions and their various degenerate cases are discussed in the asymptotic analysis. Numerical simulations are performed to support the analytical results, and the stability analysis indicates that the $\mathcal{PT}$-symmetry breaking can also destroy the stability of the soliton interactions.

DOI: 10.1103/PhysRevE.91.033202 PACS number(s): 05.45.Yv, 02.30.Ik

I. INTRODUCTION

In 1998, Bender and Boettcher pointed out that in quantum mechanics a wide class of non-Hermitian but parity-time ($\mathcal{PT}$) -symmetric Hamiltonians can possess entirely real spectra as long as the $\mathcal{PT}$ symmetry is not spontaneously broken [1]. Since then, there has been a growing interest in the non-Hermitian systems with $\mathcal{PT}$ symmetry [2–12]. Generally, the non-Hermitian Hamiltonian $H = \hat{p}^2/2 + V(x)$ is said to be $\mathcal{PT}$ symmetric if $V(x) = V^*(-x)$, where $\hat{p}$ denotes the momentum operator and $V(x)$ is the complex potential [1,2]. From an experimental viewpoint, it has been suggested that optics could provide an ideal testing ground for the unique property of such systems in view of the mathematical similarity between the paraxial equation of diffraction in optics and the Schrödinger equation in quantum mechanics [3–6]. In optics, the $\mathcal{PT}$-symmetric potential can be realized by controlling the complex refractive index distribution $n(x) = n_R(x) + in_I(x)$ [3–6], where the refractive index profile $n_R(x)$ must be an even function in the transverse direction, while the gain or loss component $n_I(x)$ should be an odd one [3–6]. Recently, the $\mathcal{PT}$-symmetry breaking within the realm of optics has been observed in experiment [6–9], and some unusual characteristics of the beam transmission in the $\mathcal{PT}$-symmetric waveguides have been revealed, such as the unidirectional invisibility [10] and nonlinear switching effect [11].

In the nonlinear optics, the nonlinear Schrödinger (NLS) equations including the Kerr nonlinearity and $\mathcal{PT}$-symmetric linear potentials have been intensively studied in the past few years [12–16]. For instance, those works include the following aspects: the interactions of bright and dark solitons with a $\mathcal{PT}$-symmetric dipole [13], the effect of competing nonlinearities on beam dynamics in $\mathcal{PT}$-symmetric potentials [12,14], stable dark solitons in $\mathcal{PT}$-symmetric dual-core waveguides [15], and dynamical behaviors in the oligomers [16]. However, the complex-valued linear potential usually breaks the integrability of the equation, so that the nonlinear beam dynamics in the presence of $\mathcal{PT}$-symmetric optical potential has been mainly studied by the numerical methods [17,18]. Moveover, the Kerr nonlinearity can dynamically induce an effective linear potential which may break the even symmetry of the real part in the $\mathcal{PT}$ potential, and further lead to the $\mathcal{PT}$-breaking instability of the beam evolution [19].

Recently, Ablowitz and Musslimani [20] proposed a nonlocal NLS equation

$$iu_z(x,z) = u_{xx}(x,z) + 2\sigma u(x,z)u^*(-x,z)u(x,z) \quad (\sigma = \pm 1), \tag{1}$$

which is non-Hermitian but $\mathcal{PT}$ symmetric, where $u(x,z)$ is a complex-valued function of real variables x and z, and $\sigma = \pm 1$ denotes, respectively, the focusing (+) and defocusing (−) cases. The nonlinear term in Eq. (1) brings a self-induced potential of the form $V(x,z) = u(x,z)u^*(-x,z)$ satisfying the $\mathcal{PT}$-symmetric condition $V(x,z) = V^*(-x,z)$. The Lax pair and an infinite number of conserved quantities have been obtained, which indicates that Eq. (1) is integrable [20]. However, the exact moving one-soliton solution obtained via the inverse scattering transform in Ref. [20] is singular for the focusing case. Although the bright and dark solitons of Eq. (1) have been obtained, both of them are static (i.e., the soliton does not propagate with distance) [19]. In addition, several periodic and hyperbolic soliton solutions have been given in Ref. [21].

Since Eq. (1) has been proved to be integrable, in this paper we will try to reveal abundant nonlinear localized-wave phenomena. On the one hand, we will apply the Nth iterated Darboux transformation (DT) to derive a chain of nonsingular localized-wave solutions that can describe the soliton interactions on the continuous-wave (cw) background. The types of soliton interactions will be discussed in detail. On the other hand, we will perform numerical simulations on the soliton interactions and study the effect of the $\mathcal{PT}$ symmetry breaking on their stability.

II. DARBOUX TRANSFORMATION FOR EQ. (1)

In this section we construct the successively iterated DT of Eq. (1). The DT, which comprises the eigenfunction and potential transformations, can be used to recursively generate

*Corresponding author: micheller85@126.com

†Corresponding author: xutao@cup.edu.cn

an infinite chain of solutions including the multisoliton solutions, periodic wave solutions, and rational solutions [22] from a trivial solution. Moreover, the DT algorithm enables us to represent the iterated solutions in terms of determinants such as the Wronskian and Grammian [22], which can further provide an algebraic basis to analyze the asymptotic behavior of the solutions [23].

The Lax pair of Eq. (1) takes the form [20]

$$\Psi_x = U\Psi = \begin{pmatrix} \lambda & u(x,z) \\ -\sigma u^*(-x,z) & -\lambda \end{pmatrix}\Psi, \tag{2a}$$

$$\Psi_z = V\Psi = \begin{pmatrix} -2i\lambda^2 - i\sigma u(x,z)u^*(-x,z) & -2i\lambda u(x,z) - iu_x(x,z) \\ 2i\sigma\lambda u^*(-x,z) + i\sigma u_x^*(-x,z) & 2i\lambda^2 + i\sigma u(x,z)u^*(-x,z) \end{pmatrix}\Psi, \tag{2b}$$

where $\Psi = (\psi_1,\psi_2)^{\mathrm{T}}$ (the superscript T signifies the vector transpose) is the vector eigenfunction, λ is the spectral parameter, and the compatibility condition $U_z - V_x + UV - VU = 0$ is exactly equivalent to Eq. (1). We assume the Nth iterated eigenfunction transformation on the Lax pair (2a) and (2b) to be of the form

$$\Psi_N = T_N\Psi, \quad T_N = \begin{pmatrix} A_N(x,z,\lambda) & B_N(x,z,\lambda) \\ C_N(x,z,\lambda) & D_N(x,z,\lambda) \end{pmatrix} \tag{3}$$

with

$$\begin{aligned} A_N(x,z,\lambda) &= \lambda^N - \sum_{n=1}^{N} a_n(x,z)\lambda^{n-1}, \\ B_N(x,z,\lambda) &= -\sum_{n=1}^{N} b_n(x,z)(-\lambda)^{n-1}, \end{aligned} \tag{4}$$

$$\begin{aligned} C_N(x,z,\lambda) &= -\sum_{n=1}^{N} c_n(x,z)\lambda^{n-1}, \\ D_N(x,z,\lambda) &= \lambda^N - \sum_{n=1}^{N} d_n(x,z)(-\lambda)^{n-1}, \end{aligned} \tag{5}$$

where T_N is the Nth iterated Darboux matrix, with $a_n(x,z)$, $b_n(x,z)$, $c_n(x,z)$, and $d_n(x,z)$ $(1 \leqslant n \leqslant N)$ to be determined, and $\Psi_N = (\psi_{1N},\psi_{2N})^{\mathrm{T}}$ is the Nth iterated eigenfunction. With the knowledge of the DT, Ψ_N is required to satisfy $\Psi_{N,x} = U_N\Psi_N$ and $\Psi_{N,z} = V_N\Psi_N$, where U_N and V_N are the same as U and V except that $u(x,z)$ and $u^*(-x,z)$ are replaced by the Nth iterated potentials $u_N(x,z)$ and $u_N^*(-x,z)$, respectively, which are also to be determined.

It is easy to find that if $\Psi_k = [f_k(x,z),g_k(x,z)]^{\mathrm{T}}$ satisfies the Lax pair (2a) and (2b) with $\lambda = \lambda_k$ $(1 \leqslant k \leqslant N)$, then $\bar{\Psi}_k = [\sigma\, g_k^*(-x,z), f_k^*(-x,z)]^{\mathrm{T}}$ is also a solution of the Lax pair (2a) and (2b) with $\lambda = \lambda_k^*$ $(1 \leqslant k \leqslant N)$ [20]. Thus, we choose Ψ_k and $\bar{\Psi}_k$ $(1 \leqslant k \leqslant N)$ as the kernel for the construction of the Nth iterated DT, that is,

$$T_N|_{\lambda=\lambda_k}\Psi_k = \mathbf{0}, \quad T_N|_{\lambda=\lambda_k^*}\bar{\Psi}_k = \mathbf{0}, \tag{6}$$

which yields the following two sets of linear equations:

$$QX_i = Y_i \quad (i = 1,2) \quad \text{with} \quad Q = \begin{pmatrix} F_{N\times N} & G_{N\times N} \\ \sigma\bar{G}_{N\times N} & \bar{F}_{N\times N} \end{pmatrix}, \tag{7}$$

where

$$\begin{aligned} X_1 &= [a_1(x,z),\ldots,a_N(x,z),b_1(x,z),\ldots,b_N(x,z)]^{\mathrm{T}}, \\ X_2 &= [c_1(x,z),\ldots,c_N(x,z),d_1(x,z)\ldots,d_N(x,z)]^{\mathrm{T}}, \\ Y_1 &= \left[\lambda_1^N f_1(x,z),\ldots,\lambda_N^N f_N(x,z),\sigma\lambda_1^{*N} g_1^*(-x,z),\ldots,\right. \\ &\quad \left.\sigma\lambda_N^{*N} g_N^*(-x,z)\right]^{\mathrm{T}}, \\ Y_2 &= \left[\lambda_1^N g_1(x,z),\ldots,\lambda_N^N g_N(x,z),\lambda_1^{*N} f_1^*(-x,z),\ldots,\right. \\ &\quad \left.\sigma\lambda_N^{*N} f_N^*(-x,z)\right]^{\mathrm{T}}, \\ F_{N\times N} &= \left[\lambda_k^{m-1} f_k(x,z)\right]_{1\leqslant k,m\leqslant N}, \\ G_{N\times N} &= [(-\lambda_k)^{m-1} g_k]_{1\leqslant k,m\leqslant N}, \\ \bar{F}_{N\times N} &= [(-\lambda_k^*)^{m-1} f_k^*(-x,z)]_{1\leqslant k,m\leqslant N}, \\ \bar{G}_{N\times N} &= [(\lambda_k^*)^{m-1} g_k^*(-x,z)]_{1\leqslant k,m\leqslant N}. \end{aligned}$$

Note that $\{\Psi_k\}_{k=1}^N$ and $\{\bar{\Psi}_k\}_{k=1}^N$ are a set of linearly independent functions because $\lambda_k \neq \lambda_l$ $(1 \leqslant k < l \leqslant N)$. That is to say, the functions $a_n(x,z)$, $b_n(x,z)$, $c_n(x,z)$, and $d_n(x,z)$ $(1 \leqslant n \leqslant N)$ can be uniquely determined from Eq. (6) by Cramer's rule. On the other hand, Eq. (7) also implies that λ_k and λ_k^* are both the single roots of $\det(T_N)$ for $1 \leqslant k \leqslant N$. Therefore, we can finally prove that the form-invariance conditions for the Lax pair (2a) and (2b),

$$T_{N,x} + T_N U = U_N T_N, \tag{8a}$$

$$T_{N,z} + T_N V = V_N T_N, \tag{8b}$$

are exactly satisfied if the Nth iterated potential transformations are given by

$$u_N(x,z) = u(x,z) + 2\frac{\tau_{N+1,N-1}}{\tau_{N,N}}, \tag{9a}$$

$$u_N^*(-x,z) = u^*(-x,z) + 2\sigma\frac{\tau_{N-1,N+1}}{\tau_{N,N}}, \tag{9b}$$

with

$$\tau_{M,2N-M} = \begin{vmatrix} F_{N\times M} & G_{N\times(2N-M)} \\ \sigma\bar{G}_{N\times M} & \bar{F}_{N\times(2N-M)} \end{vmatrix},$$

where $M = N-1$, N, or $N+1$, the block matrices $F_{N\times M}$, $G_{N\times(2N-M)}$, $\bar{G}_{N\times M}$, and $\bar{F}_{N\times(2N-M)}$ are defined as above.

The verification of the conditions (8a) and (8b) suggests that the new eigenfunction $\Psi_N = T_N\Psi$ also satisfies the Lax pair (2a) and (2b) with $u_N(x,z)$ and $u_N^*(-x,z)$ given in (9a)

and (9b) instead of $u(x,z)$ and $u^*(-x,z)$, respectively. That is to say, the eigenfunction transformation (3) and potential transformations (9a) and (9b) constitute the Nth iterated DT of Eq. (1). It should be noted that we require $\mathrm{Im}(\lambda_k) \neq 0$ for $1 \leqslant k \leqslant N$ so as to avoid the trivial iteration of the DT.

III. DARK AND ANTIDARK SOLITONS ON THE CONTINUOUS-WAVE BACKGROUND

In this section we construct the localized soliton solutions on the cw background. It is easy to find that Eq. (1) admits the plane-wave solution

$$u = \rho e^{-2i\sigma\rho^2 z + i\phi}, \tag{10}$$

where ρ and ϕ are two real parameters. Inserting Eq. (10) into the Lax pair (2a) and (2b) and taking $\lambda = \lambda_k$ $(1 \leqslant k \leqslant N)$, we obtain

$$\begin{pmatrix} f_k \\ g_k \end{pmatrix} = \begin{pmatrix} e^{(-2i\sigma\rho^2 z + i\phi)/2}(\alpha_k e^{s_k\chi_k} + \beta_k e^{-s_k\chi_k}) \\ e^{-(-2i\sigma\rho^2 z + i\phi)/2}\left(\frac{(2s_k-\lambda_k)\alpha_k}{\rho} e^{s_k\chi_k} - \frac{(2s_k+\lambda_k)\beta_k}{\rho} e^{-s_k\chi_k}\right) \end{pmatrix}, \tag{11}$$

with $s_k = \sqrt{\lambda_k^2 - \sigma\rho^2}$ and $\chi_k = x - 2i\lambda_k z$, where α_k and β_k $(1 \leqslant k \leqslant N)$ are nonzero complex parameters. Then, with substitution of (11) into the potential transformations (9a) and (9b), a series of exact solutions can be derived for different choices of N. In order to obtain the localized solitonic structure, we must impose s_k $(1 \leqslant k \leqslant N)$ to be real numbers, which is satisfied only when $\sigma = -1$, $\mathrm{Re}(\lambda_k) = 0$, and $0 < |\mathrm{Im}(\lambda_k)| < \rho$. In the following, we use the subscripts R and I to denote the real and imaginary parts of λ_k, respectively.

With $N = 1$, if $\lambda_{1R} = 0$ and $0 < |\lambda_{1I}| < \rho$, the solution (9a) can be written as

$$u = \rho e^{2iz\rho^2 + i\phi}\left[1 - \frac{2\lambda_{1I}(e^{2s_1\chi_1} + \gamma_1)(\kappa_1 e^{-2s_1\omega_1} + \kappa_1^*\gamma_1^*)}{\rho^2 e^{2s_1(\chi_1-\omega_1)} + \lambda_{1I}\kappa_1\gamma_1 e^{-2s_1\omega_1} + \lambda_{1I}\kappa_1^*\gamma_1^* e^{2s_1\chi_1} + |\gamma_1|^2\rho^2}\right], \tag{12}$$

where $\chi_1 = x + 2\lambda_{1I}z$, $\omega_1 = x - 2\lambda_{1I}z$, $\kappa_1 = \lambda_{1I} - is_1$, $s_1 = \sqrt{\rho^2 - \lambda_{1I}^2}$, and $\gamma_1 = \beta_1/\alpha_1$. It can be proved that the solution (12) has no singularity if and only if the following condition is satisfied:

$$\mathrm{Im}(\gamma_1\kappa_1) \neq 0 \quad \text{or} \quad \mathrm{sgn}(\lambda_{1I})\mathrm{Re}(\gamma_1\kappa_1) > 0. \tag{13}$$

To better understand the solitonic behavior in the solution (12) under the condition (13), we make an asymptotic analysis as follows.

(i) Along the line $x + 2\lambda_{1I}z = 0$ as $|z| \to \infty$, we have

$$u \to u_1^{\pm} = \rho e^{2i\rho^2 z + i\phi}\left[1 - \frac{2\lambda_{1I}(e^{2s_1\chi_1} + \gamma_1)}{\mu_1^{\pm} e^{2s_1\chi_1} + \nu_1^{\pm}}\right], \tag{14a}$$

$$|u|^2 \to |u_1^{\pm}|^2 = \rho^2\left[1 - \frac{2\gamma_{1I}s_1}{\mathrm{Re}(\gamma_1\kappa_1) + \mathrm{sgn}(\lambda_{1I})\rho|\gamma_1|\cosh(2s_1\chi_1 + \Delta_1^{\pm})}\right], \tag{14b}$$

with $\mu_1^- = \lambda_{1I}$, $\nu_1^- = \gamma_1\kappa_1$, $\mu_1^+ = \kappa_1^*$, $\nu_1^+ = \gamma_1\lambda_{1I}$, $\Delta_1^- = \ln\frac{|\lambda_{1I}|}{\rho|\gamma_1|}$, and $\Delta_1^+ = \ln\frac{\rho}{|\gamma_1||\lambda_{1I}|}$, where the plus sign corresponds to $\lambda_{1I} > 0$ as $z \to \infty$ or $\lambda_{1I} < 0$ as $z \to -\infty$ and the minus sign to $\lambda_{1I} < 0$ as $z \to \infty$ or $\lambda_{1I} > 0$ as $z \to -\infty$.

(ii) Along the line $x - 2\lambda_{1I}z = 0$ as $|z| \to \infty$, we have

$$u \to u_2^{\pm} = \rho e^{2i\rho^2 z + i\phi}\left[1 - \frac{2\lambda_{1I}(\kappa_1 e^{-2s_1\omega_1} + \kappa_1^*\gamma_1^*)}{\xi_1^{\pm} e^{-2s_1\omega_1} + \eta_1^{\pm}}\right], \tag{15a}$$

$$|u|^2 \to |u_2^{\pm}|^2 = \rho^2 + \frac{2s_1\mathrm{Im}(\gamma_1\kappa_1^2)}{\mathrm{sgn}(\lambda_{1I})\rho|\gamma_1|\cosh(2s_1\omega_1 - \Delta_1^{\pm}) + \mathrm{Re}(\gamma_1\kappa_1)}, \tag{15b}$$

with $\xi_1^- = \kappa_1\lambda_{1I}$, $\eta_1^- = \rho^2\gamma_1^*$, $\xi_1^+ = \rho^2$, and $\eta_1^+ = \kappa_1^*\lambda_{1I}\gamma_1^*$, where the plus sign corresponds to $\lambda_{1I} < 0$ as $z \to \infty$ or $\lambda_{1I} > 0$ as $z \to -\infty$ and the minus sign to $\lambda_{1I} > 0$ as $z \to \infty$ or $\lambda_{1I} < 0$ as $z \to -\infty$.

If $\mathrm{Im}(\gamma_1\kappa_1) \neq 0$ or $\mathrm{sgn}(\lambda_{1I})\mathrm{Re}(\gamma_1\kappa_1) > 0$, Eq. (14a) represents the antidark soliton for $\lambda_{1I}\gamma_{1I} < 0$ or dark soliton for $\lambda_{1I}\gamma_{1I} > 0$ on a cw background, while Eq. (15a) also represents the antidark soliton for $\lambda_{1I}\mathrm{Im}(\gamma_1\kappa_1^2) > 0$ or dark soliton for $\lambda_{1I}\mathrm{Im}(\gamma_1\kappa_1^2) < 0$ on the same cw background. From Eqs. (14b) and (15b) we can observe the following features. (a) The heights of the antidark solitons (or the depths of the dark solitons) from the cw background are the same for $|u_i^-|^2$ and $|u_i^+|^2$ $(i = 1,2)$, that is,

$$A_1^{\pm} = \frac{2\rho^2|\gamma_{1I}s_1|}{\mathrm{Re}(\gamma_1\kappa_1) + \mathrm{sgn}(\lambda_{1I})\rho|\gamma_1|}, \qquad A_2^{\pm} = \frac{2|s_1\mathrm{Im}(\gamma_1\kappa_1^2)|}{\mathrm{sgn}(\lambda_{1I})\rho|\gamma_1| + \mathrm{Re}(\gamma_1\kappa_1)}. \tag{16}$$

(b) The envelope velocity of u_i^- is also exactly equal to that of u_i^+ $(i = 1,2)$, i.e., $v_1^- = v_1^+ = -2\lambda_{1I}$ and $v_2^- = v_2^+ = 2\lambda_{1I}$. (c) There exists a phase shift between u_i^- and u_i^+ $(i = 1,2)$ and its absolute value can be calculated by $|\Delta_1^+ - \Delta_1^-| =$

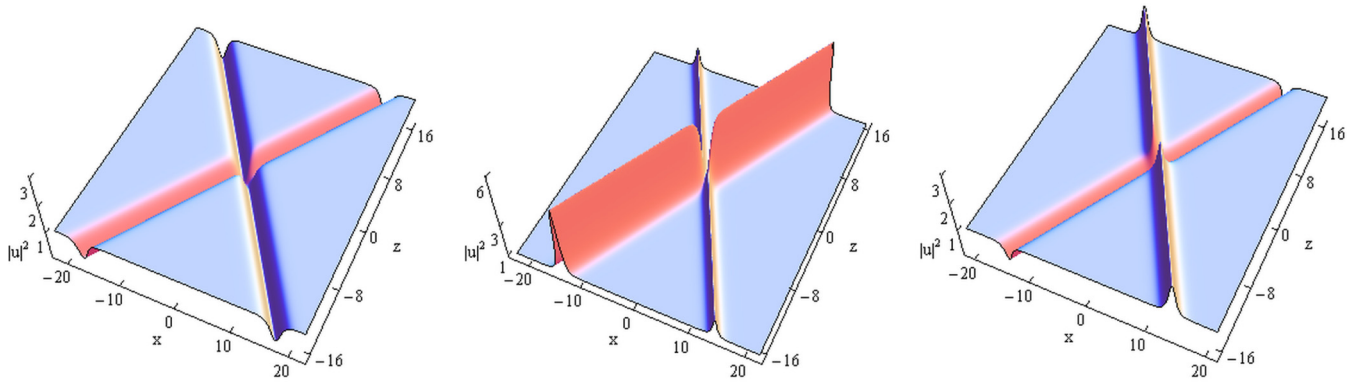

FIG. 1. (Color online) Elastic interactions via the solution (12) between (a) two dark solitons with $\rho = 1, \lambda_1 = -0.5\,i$, and $\gamma_1 = 0.4 - 0.5\,i$; (b) two antidark solitons with $\rho = 1$, $\lambda_1 = 0.4\,i$, and $\gamma_1 = -2 - 0.5i$; and (c) dark and antidark solitons with $\rho = 1$, $\lambda_1 = 0.4\,i$, and $\gamma_1 = 1 - 0.6i$.

$2|\ln \frac{\rho}{|\lambda_{1I}|}|$, which means that the phase shift depends on both ρ and λ_{1I}.

The above three features suggest that the solution (12) under the condition (13) can describe the elastic two-soliton interactions on the cw background. To be specific, the elastic interactions may occur between two dark solitons, two antidark solitons, or dark and antidark solitons, as shown in Figs. 1(a)–1(c). In any of the three kinds of interactions, the interacting solitons can completely recover their individual shapes and velocities upon an interaction and experience only the phase shifts for their envelops. Particularly taking $\gamma_{1I} = 0$, the pair of asymptotic solitons (u_1^-, u_1^+) disappears as $z \to \pm\infty$, but (u_2^-, u_2^+) still exists and represent a pair of antidark solitons for $\gamma_{1R} > 0$ or dark solitons for $\gamma_{1R} < 0$ [see Fig. 2(a)]. However, the solution (12) in this degenerate case cannot be regarded as the conventional single soliton because there exists a phase shift between the soliton envelopes of u_2^- and u_2^+. Similarly, for the degenerate case $\mathrm{Im}(\gamma_1\kappa_1^2) = 0$, one can find that only the pair of asymptotic solitons (u_1^-, u_1^+) exists as $|z| \to \infty$ and there is also a phase shift between u_1^- and u_1^+ [see Fig. 2(b)]. Associated with $\lambda_{1I}\gamma_{1I} < 0$ and $\lambda_{1I}\gamma_{1I} > 0$, (u_1^-, u_1^+) can represent a pair of antidark solitons and a pair of dark solitons, respectively. In Table I we present all possible types of soliton interactions in the solution (12) and their associated parametric conditions.

If $\lambda_{kR} = 0$ and $0 < |\lambda_{kI}| < \rho$ for $k = 1,2$, the solution (9a) with $N = 2$ can describe abundant soliton interactions on the cw background. In this case, the solution has in general four pairs of asymptotic solitons along four lines $x \pm 2\lambda_{kI} z = 0$ $(k = 1,2)$ as $|z| \to \infty$. The expressions of asymptotic soliton pairs along $x + 2\lambda_{kI} z = 0$ and $x - 2\lambda_{kI} z = 0$, respectively, have the same form of Eqs. (14a) and (14b) but for some difference in the parameters (details are omitted to save space). Therefore, each pair of asymptotic solitons as $z \to \pm\infty$ could be either dark or antidark ones depending on the different parametric choices. Moreover, they have the same shapes, velocities, and intensities and differ only by the phases of their envelopes, which satisfies the standard of elastic interactions. For example, Figs. 3(a)–3(c) present three different types of elastic four-soliton interactions. In addition, if $\gamma_{kI} = 0$ or $\mathrm{Im}(\gamma_k\kappa_k^2) = 0$ $(k = 1,2)$, some asymptotic solitons will disappear as $z \to \pm\infty$, so the four-soliton interactions degenerate to the three-soliton interactions and even two-soliton interactions, as shown in Figs. 4(a)–4(c).

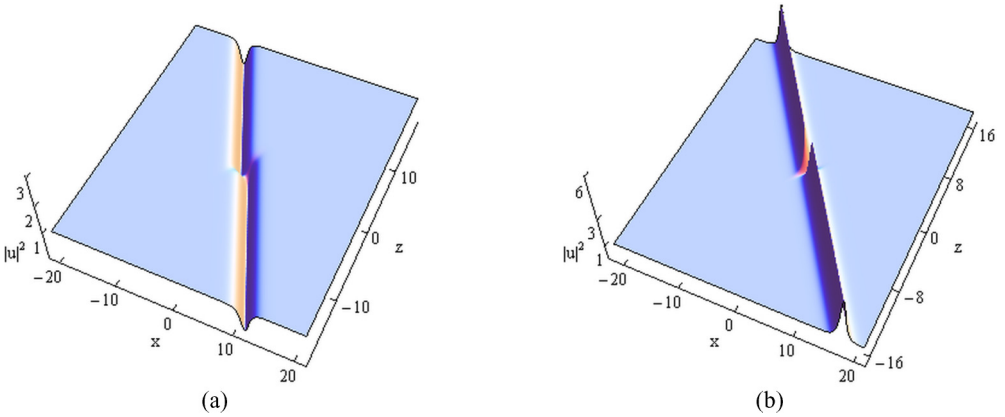

FIG. 2. (Color online) Degenerate two-soliton interactions via the solution (12): (a) dark soliton that has a phase shift between two soliton segments as $z \to \pm\infty$, where $\rho = 1$, $\lambda_1 = -0.3\,i$, and $\gamma_1 = 1$, and (b) antidark soliton that has a phase shift between two soliton segments as $z \to \pm\infty$, where $\rho = 1$, $\lambda_1 = 0.5\,i$, and $\gamma_1 = 2/\sqrt{3} - 2i$.

TABLE I. Asymptotic patterns of the solution (12) under different parametric conditions.

Parametric conditions	Asymptotic soliton $u_1^{\pm}$	Asymptotic soliton $u_2^{\pm}$
$\lambda_{1I}\gamma_{1I} > 0, \lambda_{1I}\mathrm{Im}(\gamma_1\kappa_1^2) < 0$	dark soliton	dark soliton
$\lambda_{1I}\gamma_{1I} < 0, \lambda_{1I}\mathrm{Im}(\gamma_1\kappa_1^2) > 0$	antidark soliton	antidark soliton
$\lambda_{1I}\gamma_{1I} < 0, \lambda_{1I}\mathrm{Im}(\gamma_1\kappa_1^2) < 0$	antidark soliton	dark soliton
$\lambda_{1I}\gamma_{1I} > 0, \lambda_{1I}\mathrm{Im}(\gamma_1\kappa_1^2) > 0$	dark soliton	antidark soliton
$\gamma_{1I} = 0, \gamma_{1R} < 0$	disappear	dark soliton
$\gamma_{1I} = 0, \gamma_{1R} > 0$	disappear	antidark soliton
$\mathrm{Im}(\gamma_1\kappa_1^2) = 0, \lambda_{1I}\gamma_{1I} < 0$	antidark soliton	disappear
$\mathrm{Im}(\gamma_1\kappa_1^2) = 0, \lambda_{1I}\gamma_{1I} > 0$	dark soliton	disappear

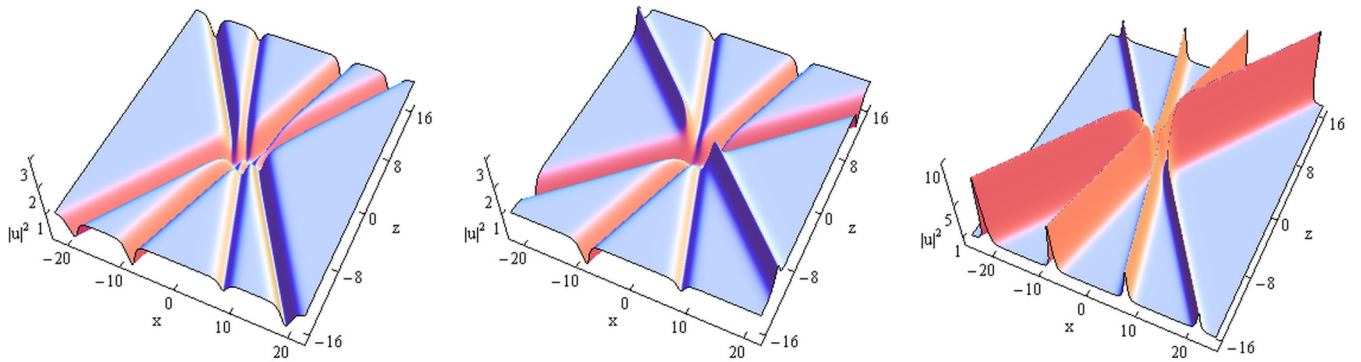

FIG. 3. (Color online) Elastic interactions among (a) four dark solitons with $\rho = 1$, $\phi = 0$, $\gamma_1 = 1 + 2i$, $\gamma_2 = 1 + i$, $\lambda_1 = 0.5\,i$, and $\lambda_2 = -0.25\,i$; (b) three dark solitons and one antidark solitons with $\rho = 1$, $\phi = 0$, $\gamma_1 = 1 - i$, $\gamma_2 = 1 + i$, $\lambda_1 = 0.8\,i$, and $\lambda_2 = -0.25\,i$; and (c) four antidark solitons with $\rho = 1$, $\phi = 0$, $\gamma_1 = 1.5 + i$, $\gamma_2 = i$, $\lambda_1 = 0.2\,i$, and $\lambda_2 = -0.6\,i$.

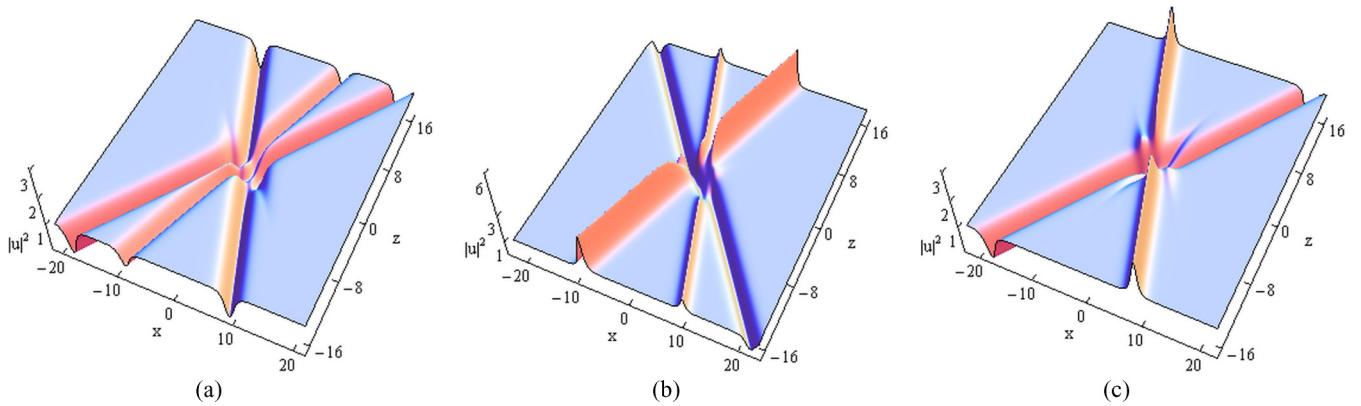

FIG. 4. (Color online) Degenerate four-soliton interactions via the solution (9a) with $N = 2$: (a) elastic interactions among three dark solitons with $\rho = 1$, $\phi = 0$, $\gamma_1 = 1$, $\gamma_2 = 1 - 2i$, $\lambda_1 = 0.5\,i$, and $\lambda_2 = 0.25\,i$; (b) elastic interactions among one dark soliton and two antidark solitons with $\rho = 1$, $\phi = 0$, $\gamma_1 = 1$, $\gamma_2 = 4 + i$, $\lambda_1 = -0.6\,i$, and $\lambda_2 = 0.25\,i$; and (c) elastic interactions between dark and antidark solitons with $\rho = 1$, $\phi = 0$, $\gamma_1 = 2$, $\gamma_2 = 0.5$, $\lambda_1 = -0.25\,i$, and $\lambda_2 = 0.5\,i$.

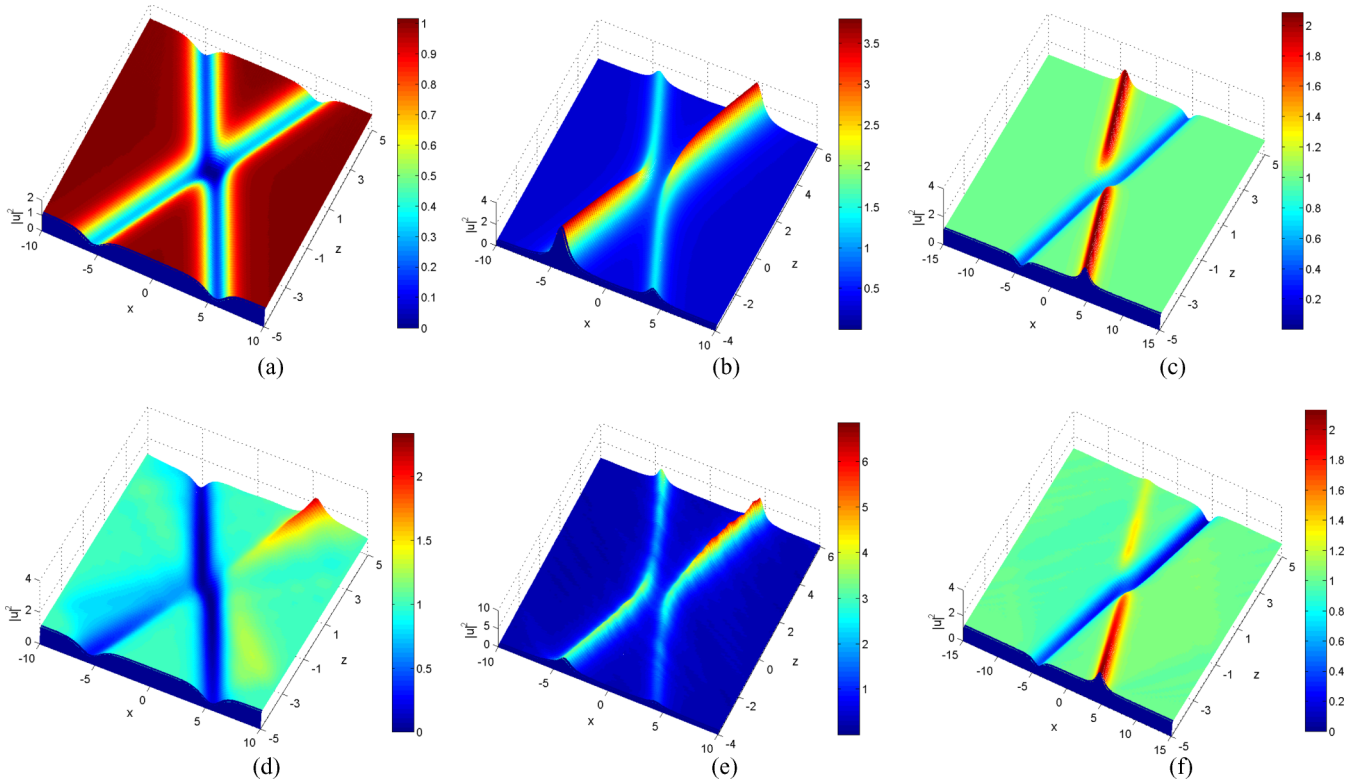

FIG. 5. (Color online) Numerical simulations of the elastic two-soliton interactions with initial value $u(x,-5)$ in Eq. (17), where the parameters are the same as those in Fig. 2: (a) two dark solitons, (b) two antidark solitons, (c) dark and antidark solitons, (d) unstable case of (a) with a 0.1 shift, (e) unstable case of (b) with a 0.1 shift, and (f) unstable case of (c) with a 0.02 shift.

IV. NUMERICAL SIMULATIONS AND $\mathcal{PT}$-SYMMETRY BREAKING

It has been suggested in Ref. [19] that the stability of the solutions of Eq. (1) may be influenced by the shift in the transverse coordinate. In contrast with the standard NLS equation, the self-induced potential in Eq. (1), i.e., $V(x,z) = u(x,z)u^*(-x,z)$, can break its $\mathcal{PT}$ symmetry if the square modulus of the solution $u(x,z)$ is not symmetric in the transverse coordinate x or the imaginary part increases beyond a certain threshold. The breaking of $\mathcal{PT}$ symmetry will lead to the instability of the solution. In Ref. [19], the static bright and dark one-soliton solutions have been shown to be unstable due to the spontaneous $\mathcal{PT}$-symmetry breaking. In this section, numerical simulations of Eq. (1) are performed by using the time-splitting spectral (TSS) method to support the theoretical analysis in Secs. II and III and to analyze the instability of the soliton interactions caused by the $\mathcal{PT}$-symmetry breaking.

For the numerical experiments, we choose $u(x,z)$ in the solution (12) at $z = -5$ as the initial value:

$$u(x,-5) = \rho e^{-10i\rho^2+i\phi}\left[1 - \frac{2\lambda_{1I}(e^{2s_1\chi_1}+\gamma_1)(\kappa_1 e^{-2s_1\omega_1}+\kappa_1^*\gamma_1^*)}{\rho^2 e^{2s_1(\chi_1-\omega_1)} + \lambda_{1I}\kappa_1\gamma_1 e^{-2s_1\omega_1} + \lambda_{1I}\kappa_1^*\gamma_1^* e^{2s_1\chi_1} + |\gamma_1|^2\rho^2}\right], \tag{17}$$

where $\chi_1 = x - 10\lambda_{1I}$, $\omega_1 = x + 10\lambda_{1I}$, and κ_1, s_1, and γ_1 are the same as those in the solution (12). When the parameters are the same as those in Fig. 1(a), the initial value corresponds to two well-separated dark solitons with different incident angles. Through the TSS numerical method, we find that those two dark solitons pass through each other without any change except for the small shift [see Fig. 5(a)], which is consistent with the theoretical analysis in Fig. 1(a). Similarly, with the parametric choice in Figs. 1(b) and 1(c), the stable interactions between two antidark solitons and between dark and antidark solitons are desmonstrated in Figs. 5(b) and 5(c), respectively. However, when the initial value in Eq. (17) has a small shift in the x coordinate the $\mathcal{PT}$ symmetry will break and those three types of interactions between two solitons will be unstable. For the dark-dark soliton interaction case with a 0.1 shift in the x coordinate, Fig. 5(d) shows that the depth of the dark soliton on the minus axis is smaller than that in Fig. 5(a) before the interaction, while after the interaction the soliton becomes an antidark one and the amplitude grows rapidly. For the case of two antidark soliton interaction with a 0.1 shift in the x coordinate, the amplitudes of the two solitons get enhanced after the interaction, as shown in Fig. 5(e). In addition, if we only make a 0.02 shift for the dark-antidark soliton interaction, there still exists an obvious instability: The

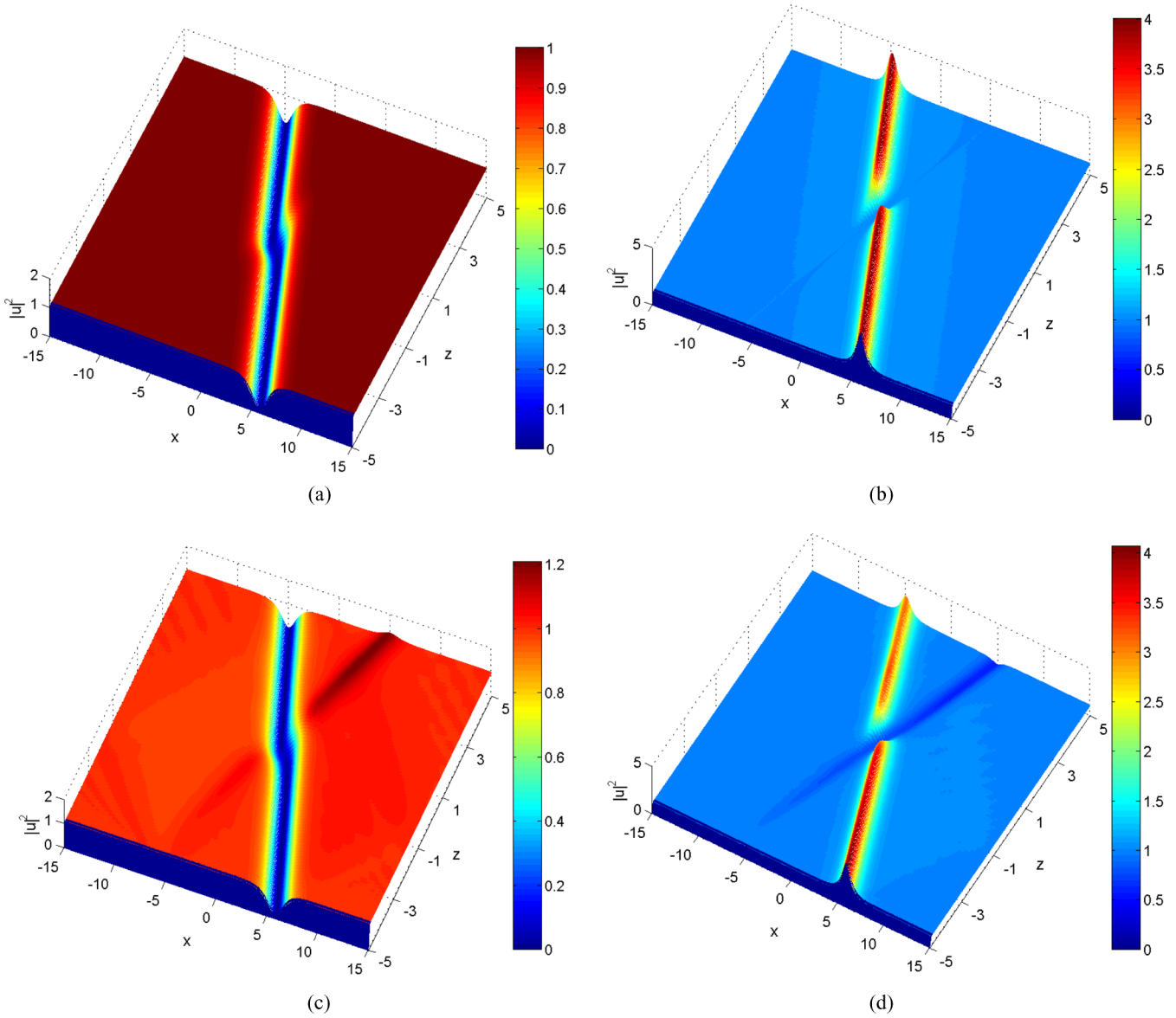

FIG. 6. (Color online) Numerical simulations of the degenerated cases of two-soliton interactions with initial value $u(x, -5)$ in Eq. (17), where the parameters are the same as those in Fig. 3: (a) dark soliton, (b) antidark soliton, (c) unstable case of (a) with a 0.01 shift, and (d) unstable case of (b) with a 0.01 shift.

depth of the dark soliton increases while the amplitude of the antidark one decreases as the distance z evolves, as shown in Fig. 5(f).

For the degenerate cases of two-soliton interactions, the stable propagation of a dark soliton and an antidark soliton are also simulated in Figs. 6(a) and 6(b) by choosing the same parameters as in Figs. 2(a) and 2(b), respectively. Although one soliton can disappear by taking particular parametric values, the remaining soliton is not the conventional single soliton because there is a phase shift between the two segments as $z \to \pm\infty$. When the initial value in solution (17) is shifted slightly in the x coordinate, Figs. 6(c) and 6(d) show that the $\mathcal{PT}$-symmetry breaking stimulates the disappearing soliton and makes the propagation of the remaining one unstable. The numerical analysis of the three-soliton interactions can be performed similarly (details are omitted for brevity). Those simulations above not only support the theoretical analysis in Secs. II and III, but also show that the $\mathcal{PT}$-symmetry breaking can lead to instability of the soliton interactions.

V. CONCLUSION

In this paper we have studied the nonlinear localized-wave phenomena on the cw background for a nonlocal NLS equation with the self-induced $\mathcal{PT}$-symmetric potential [i.e., Eq. (1)]. We have constructed the Nth iterated DT of Eq. (1) and derived a chain of nonsingular localized-wave solutions starting from a plane-wave solution. With $N = 1$, we have obtained the solution (12), which describes the two-soliton interactions on the cw background. Through asymptotic analysis, we have presented several types of two-soliton interactions (e.g., between two dark, two antidark, and dark and antidark

solitons), as shown in Fig. 1. In particular, we have found that one of the asymptotic solitons can disappear as $|z| \to \infty$ under the degenerate parametric conditions, as shown in Fig. 2, and the remaining dark or antidark soliton undergoes a phase shift, which is different from the conventional single soliton. The associated parametric conditions for all possible types of soliton interactions in the solution (12) have been given in Table I. Similarly, with $N = 2$, the four-soliton interactions and their various degenerate cases (three- and two-soliton interactions) have been analyzed in Figs. 3 and 4, respectively. Finally, numerical simulations of the soliton interactions have been performed, which shows that the $\mathcal{PT}$-symmetry breaking can destroy the stability of the soliton interactions, as shown in Figs. 5 and 6.

We can infer that the Nth iterated solution in general exhibits a variety of elastic interactions among $2N$ solitons on the cw background and each interacting soliton could be of the dark or antidark type. The interactions with an arbitrary odd number of solitons can also be obtained under different degenerate conditions. If the initial value has no shift in the x coordinate, those solitons can have stable interactions on the cw background; otherwise, the $\mathcal{PT}$ symmetry will break and the soliton interaction strucures become unstable.

ACKNOWLEDGMENTS

This work was supported by the Fundamental Research Funds of the Central Universities (Projects No. 2014QN30 and No. 2014ZZD10) and by the National Natural Science Foundations of China (Grants No. 11426105, No. 11371371, No. 11305060, and No. 11271126).

[1] C. M. Bender and S. Boettcher, Phys. Rev. Lett. **80**, 5243 (1998).
[2] C. M. Bender, D. C. Brody, H. F. Jones, and B. K. Meister, Phys. Rev. Lett. **98**, 040403 (2007).
[3] D. N. Christodoulides, F. Lederer, and Y. Silberberg, Nature (London) **424**, 817 (2003).
[4] R. El-Ganainy, K. G. Makris, D. N. Christodoulides, and Z. H. Musslimani, Opt. Lett. **32**, 2632 (2007).
[5] K. G. Makris, R. El-Ganainy, D. N. Christodoulides, and Z. H. Musslimani, Phys. Rev. Lett. **100**, 103904 (2008).
[6] C. E. Ruter, K. G. Makris, R. El-Ganainy, D. N. Christodoulides, M. Segev, and D. Kip, Nat. Phys. **6**, 192 (2010).
[7] A. Guo, G. J. Salamo, D. Duchesne, R. Morandotti, M. Volatier-Ravat, V. Aimez, G. A. Siviloglou, and D. N. Christodoulides, Phys. Rev. Lett. **103**, 093902 (2009).
[8] M.-A. Miri, A. Regensburger, U. Peschel, and D. N. Christodoulides, Phys. Rev. A **86**, 023807 (2012).
[9] A. Regensburger, C. Bersch, M. A. Miri, G. Onischchukov, D. N. Christodoulides, and U. Peschel, Nature (London) **488**, 167 (2012).
[10] Z. Lin, H. Ramezani, T. Eichelkraut, T. Kottos, H. Cao, and D. N. Christodoulides, Phys. Rev. Lett. **106**, 213901 (2011).
[11] H. Ramezani, T. Kottos, R. El-Ganainy, and D. N. Christodoulides, Phys. Rev. A **82**, 043803 (2010).
[12] Z. H. Musslimani, K. G. Makris, R. El-Ganainy, and D. N. Christodoulides, Phys. Rev. Lett. **100**, 030402 (2008).
[13] N. Karjanto, W. Hanif, B. A. Malomed, and H. Susanto, arXiv:1401.4241.
[14] A. Khare, S. M. Al-Marzoug, and H. Bahlouli, Phys. Lett. A **376**, 2880 (2012).
[15] Yu. V. Bludov, V. V. Konotop, and B. A. Malomed, Phys. Rev. A **87**, 013816 (2013).
[16] M. Duanmu, K. Li, R. L. Horne, P. G. Kevrekidis, and N. Whitaker, Philos. Trans. R. Soc. London Ser. A **371**, 20120171 (2013).
[17] S. Nixon, L. J. Ge, and J. K. Yang, Phys. Rev. A **85**, 023822 (2012).
[18] Y. He, X. Zhu, D. Mihalache, J. L. Liu, and Z. X. Chen, Phys. Rev. A **85**, 013831 (2012).
[19] A. K. Sarma, M.-A. Miri, Z. H. Musslimani, and D. N. Christodoulides, Phys. Rev. E **89**, 052918 (2014).
[20] M. J. Ablowitz and Z. H. Musslimani, Phys. Rev. Lett. **110**, 064105 (2013).
[21] A. Khare and A. Saxena, arXiv:1405.5267.
[22] V. B. Matveev and M. A. Salle, *Darboux Transformations and Solitons* (Springer, Berlin, 1991).
[23] T. Xu and B. Tian, J. Phys. A **43**, 245205 (2010); J. Math. Phys. **51**, 033504 (2010).